IR-pump - X-ray-probe spectroscopy of vibrationally excited molecules

Nina Ignatova,[1,2] Vinícius V. da Cruz,[2] Rafael C. Couto,[2,3] Emilie Ertan,[4] Michael Odelius,[4] Hans Ågren,[2] Freddy F.Guimarães,[3] Andrey Zimin,[1,2] Sergey Polyutov,[1] Faris Gel'mukhanov,[2,1] and Victor Kimberg[2,1]

[1]*Laboratory for Nonlinear Optics and Spectroscopy, Siberian Federal University 660041 Krasnoyarsk, Russia*

[2]*Theoretical Chemistry and Biology, Royal Institute of Technology 10691 Stockholm, Sweden*

[3]*Instituto de Química, Universidade Federal de Goiás, Campus Samambaia, CP 131 CEP 74001-970, Goiânia-GO, Brasil*

[4]*Department of Physics, Stockholm University, AlbaNova University Center, 10691 Stockholm Sweden*

(Dated: October 7, 2016)

Abstract

In the present paper we propose and discuss infrared (IR) pump x-ray probe scheme for molecular studies. We illustrate advantages of the pump-probe x-ray spectroscopy by means of numerical simulations employing vibrational wave-packet dynamics. Our study focuses on theoretical description of x-ray absorption (XAS) and resonant inelastic x-ray scattering (RIXS) spectra of molecules vibrationally excited by a preceding IR field, using the dissociative $1a_1^{-1}4a_1$ and bound $1a_1^{-1}2b_2$ core-excited states of the water molecule as demonstration cases. By choosing an initially excited vibrational state one can manipulate the wave-packet dynamics in the core-excited state and thus to control the vibrational excitations in the final state of the RIXS process. We show that the pump-probe technique allows us to study vibrational features in the core-excited state inaccessible in conventional x-ray spectroscopy due to strict selection rules in symmetric molecules. We propose here to use XAS measurements in the x-ray Raman mode as a tool to study absorption from a selected vibrational level of the ground state even in the case when the selective excitation cannot be reached by the IR pumping. The proposed technique have potential applications for an advanced mapping of multidimensional potential energy surfaces of the ground and core-excited molecular states, symmetry resolved spectroscopy and steering chemical reactions across transition state barriers.

I. INTRODUCTION

Infrared (IR) and x-ray spectroscopy, widely used for molecular studies, each have merits and limitations when applied for a particular purpose. IR spectroscopic techniques allow to measure ro-vibrational levels of the molecular electronic ground state at ultrahigh resolution. Numerous techniques have been developed for studies of the potential energy surfaces (PESs) in polyatomic systems making use of IR radiation [1]. For instance, the technique can be employed to directly map potential energy curves of diatomic molecules using the Rydberg-Klein-Rees method [2]. A disadvantage of conventional IR spectroscopy is that only few low-lying vibrational levels can be populated as the IR field becomes off-resonant for higher excitation due to anharmonisity of the PES. In order to reach a higher energy region of the PES more complex techniques using double- and triple-excitation schemes must be applied [3]. However, even in that case only a part of vibrational states can be addressed due to strong selection rules in symmetric systems.

X-rays, which address transitions of the core-electrons, are widely used to study core-excited and valence excited states with the help of x-ray absorption spectroscopy (XAS) and resonant inelastic x-ray scattering (RIXS)[4]. Due to the high element selectivity of the core orbitals, the x-ray techniques can be applied for site-selective studies of complex systems. Thanks to recent progress in the development of high-resolution x-ray spectrometers vibrationally resolved spectra can be measured that reveal complex ultrafast nuclear dynamics in the intermediate core-excited and final states of the Raman process [5]. The RIXS scheme can also successfully be applied for advanced studies of the molecular ground states, where highly excited vibrational levels are reached in the course of the evolution in the core-excited state [6–8]. However, in symmetric systems, like the water molecule, selection and propensity rules apply, and only a particular group of the vibrational levels can be excited in XAS and RIXS [6].

In the present paper, we propose a technique which combines both IR and x-ray excitation of molecules. The pump-probe method discussed here is two-step. First, the molecule is prepared by an IR pulse which creates population of the excited vibrational levels in the electronic ground state. At the second step, the molecule is probed with x-rays using XAS and RIXS schemes. A similar scheme was discussed previously [9] in terms of phase-sensitive x-ray absorption driven by strong IR fields [10]. In this case, coherent superposition of

vibrational states – the nuclear wave-packet – is created and its dynamics in the ground electronic state is probed be means of x-ray absorption spectroscopy [11]. In contrast, in this work we study changes in XAS and RIXS spectra when the process starts from a single excited vibrational state. The proposed method is applied to the water molecule, in the x-ray spectral region near the two lowest core-excited states of dissociative $1a_1^{-1}4a_1$ and bound $1a_1^{-1}2b_2$ character [12, 13]. We show advantages of the proposed schemes with the help of numerical simulations using two-dimensional wave packet techniques [14, 15] combined with high level *ab initio* calculations of the PESs. We conclude that XAS from a vibrationally excited molecule allows to probe an extended region of the core-excited PES, accordingly to the reflection principle [16]. Moreover, the antisymmetric stretching mode, which is not accessible in the convenient XAS technique, can be resolved in IR pump-XAS probe spectroscopy by core-excitation from the excited antisymmetric vibrational wave function of the ground state. Our simulation results for the symmetric H_2O molecule are compared with the non-symmetric HDO system in order to gain more information. It is clear that RIXS from a vibrationally excited molecule allows to control the final state vibrational excitation via selection of the initial vibrational wave function symmetry. Moreover, a highly excited initial state allows us to probe a wider energy range of the final state PES. In the present paper we focus on the RIXS process leading back to the ground electronic state, so providing an efficient tool for the study the ground state PES with symmetry resolution, complementary to IR spectroscopy. We assume that a single vibrational state is excited by the IR pump radiation. The state-selective vibrational excitation can be reached using the stimulated Raman process with two coherent IR pulses [17–19], or with the help of specially prepared strong $\sin^2$-shaped laser pulses [20]. In a general case, however, several vibrational levels in the ground electronic state may be populated, which results in a rather complex x-ray absorption profile as a superposition of the XAS from several initial vibrational states. In this study we provide a method to single out a partial XAS cross section from a particular vibrational state using x-ray absorption in the x-ray Raman mode (XASRM)[21], following the intensity of a selected vibrational resonance in RIXS while changing the x-ray excitation energy. We show, that the use of anti-Stokes peaks in RIXS allows for additional symmetry selection of partial XAS profiles in XASRM.

As a proof-of-principle theoretical study, we focus here on a rather simple system, gas phase water, where we show clear advantages of the vibrationally excited x-ray spectroscopy

for the symmetry control of vibrational excitation by choosing a proper initial vibrationally excited state with potential applications for the PESs reconstructions along a selected mode. The IR-x-ray pump-probe technique can, however, be adapted for study of rather complex systems, for example, as a powerful complementary tool reinforcing existing attempts of probing the local structure of the liquid water, or for an advanced control over nuclear dynamics of the reactions going through the energy barrier.

The paper is organized as follows. In Sec. II we present our theoretical approach for *ab initio* electronic structure and nuclear wave packet simulations. Sec. III discusses our results for XAS (Sec. III A), RIXS (Sec. III B) and XASRM (Sec. III C). Our fundings are summarized in Sec. IV.

II. THEORY

The studied gas phase water molecule has three vibrational degrees of freedom: symmetric and antisymmetric stretching, and bending modes with vibrational quanta $\omega_s = 0.4531$ eV, ω_a=0.4654 eV, ω_b=0.1976 eV [22], respectively. In the ground electronic state, the two stretching modes are nearly degenerate and strongly coupled via Darling-Dennison coupling [23–25], which have to be considered together for a proper system description. In contrast, the bending mode is only weakly coupled to the stretching modes, and can thus be considered separately in an orthonormal approximation [15]. Previous studies [15, 26] have shown that the bending mode is only weakly excited in XAS and RIXS near the two lowest core-excited states. Due to this circumstance, we neglect here the bending motion and focus fully on the two coupled stretching modes using a two-dimensional (2D) approach, as described below. Summarizing, in the present work we study the water molecule with two-step pump-probe spectroscopy: 1) an IR pulse populates a particular vibrational level of the electronic ground state, 2) the following x-ray photon promotes an oxygen 1s electron to the LUMO and LUMO+1 molecular orbitals, referred in the paper as the $4a_1$ and $2b_2$ core-excited states, respectively. The XAS and RIXS spectra of the vibrationally excited molecule are computed and discussed.

A. 2D approach for coupled stretching modes

For the coupled stretching modes picture the 2D vibrational wave functions can be assigned as $\psi_{s,a}$, where the indices s, a describe the symmetric and antisymmetric vibrational excited quantum (s, a). The initial vibrational excitation can be achieved with the help of an IR field resonant to the vibrational transition in the ground electronic state. When the IR field is weak only the first vibrational levels (10) and (01) are populated, since the vibrational quanta of symmetric and antisymmetric modes of the ground state water molecule are nearly degenerate. The higher vibrational levels are populated by a ladder-type process when the intensity of the IR laser is sufficiently high. Due to presence of quasi-degeneracy in the levels of each vibrational group $n = s + a$, the vibrational levels are populated in the groups according to the following scheme: $(00) \rightarrow (10), (01) \rightarrow (20), (11), (02) \cdots$. The strength of each IR transition is defined by the **R**-dependence of the permanent dipole moment d in the ground electronic state

$$d'_{Q_s}\langle\psi_{s,a}|Q_s|\psi_{s\pm1,a}\rangle, \quad d'_{Q_a}\langle\psi_{s,a}|Q_a|\psi_{s,a\pm1}\rangle, \tag{1}$$

where $d'_{Q_{s,a}}$ is the derivative of the dipole moment over the normal coordinate $Q_{s,a}$ at the equilibrium.

The PESs for the ground, and the two lowest $4a_1$ [12, 13] and $2b_2$ [13] core-excited states were computed at the RASSCF (restricted active space self-consistent field) theory level[27] implemented in the MOLCAS package[28] (see Fig. 1(b)). Computational details can be found in our previous RIXS study of the vibrationally cold water molecule [15] which confirms the applicability of the model. The normal mode picture describes well the vibrational dynamics near the equilibrium. However, it fails for the higher excited vibrational states because of strong anharmonicity of the two-dimensional PESs. Due to this fact we choose to use valence coordinates (R_1, R_2, θ, see Fig. 1(a)) instead of normal mode coordinates for our numerical simulations. Using valence coordinates, we consider the Hamiltonian of the 2D stretching motion in the n-th electronic state as

$$h_n = -\frac{1}{2\mu_1}\frac{\partial^2}{\partial R_1^2} - \frac{1}{2\mu_2}\frac{\partial^2}{\partial R_2^2} - \frac{\cos\theta_0}{m_O}\frac{\partial^2}{\partial R_1 \partial R_2} + V_n(R_1, R_2, \theta_0) \tag{2}$$

where θ_0 is the equilibrium bond angle, $\mu_\alpha = m_\alpha m_O/(m_\alpha + m_O)$ is the reduced mass with $\alpha = 1, 2$, and $V_n(R_1, R_2, \theta)$ is the potential energy of the n-th electronic state, defined

with respect to its minimum. For the water molecule $\mu_1 = \mu_2 = \mu_H$, while for isotopic substitution of water HDO, studied here as well, $\mu_1 = \mu_H$ and $\mu_2 = \mu_D$. In order to compute the XAS and RIXS profiles we employ the time-dependent wave packet formalism [29] in the 2D representation [6, 15] with the Hamiltonian (2), as it is described in the following subsections.

B. X-ray absorption of vibrationally excited molecules

When the ground state is excited by an IR pulse, the x-ray absorption cross section reads

$$\sigma_{\rm abs}(\omega) = \int_0^\infty dt\; e^{(\imath(\Omega+\Delta)-\Gamma)t}\sigma(t), \quad \sigma(t) = \langle\psi_\nu|\Psi_c(t)\rangle. \tag{3}$$

Here $\Omega = \omega - \omega_{\rm vert} + \epsilon_0$ is the detuning from the top of the absorption resonance, ϵ_0 is the vibrational energy of the initial vibrationally excited state $|\psi_\nu\rangle \equiv \psi_{s,a}$ ($\nu = (s,a)$) of the ground electronic state, and $\Gamma = 0.08$ eV is the lifetime broadening of the core-excited state [30]. The vertical transition energy $\omega_{\rm vert}$ and the energy relative to the PES minima Δ are defined as follows:

$$\omega_{\rm vert} = V_c(\mathbf{R}_0) - V_0(\mathbf{R}_0), \quad \Delta = V_c(\mathbf{R}_0) - V_c(\mathbf{R}_0^{(c)}), \tag{4}$$

where $\mathbf{R}_0(R_1^{(0)}, R_2^{(0)})$ and $\mathbf{R}_0^{(c)} = (R_1^{(c)}, R_2^{(c)})$ are the coordinates of the minima of the ground and core-excited states, respectively, and V_0 (V_c) is the potential energy of the ground (core-excited) state. The 2D core-excited wave packet in (3) can be computed as

$$|\Psi_c(t)\rangle = e^{-\imath h_c}|\psi_\nu\rangle, \tag{5}$$

with the Hamiltonian h_c defined according to (2), and with the initial condition $|\psi_\nu\rangle \equiv \psi_{s,a}$ as the wave function of the vibrationally excited ground state.

C. Resonant inelastic x-ray Raman scattering of vibrationally excited molecules

We consider a "quasi-elastic" scattering process, in which the system relaxes, after the core-excitation, to the electronic ground but vibrationally excited state. In this case, we deal with vibrationally inelastic x-ray Raman scattering. We compute the cross section [4]

of the RIXS process as a half-Fourier transform

$$\sigma(\omega',\omega) = P_f \mathrm{Re} \int_0^\infty dt \quad e^{\imath(\omega-\omega'+\epsilon_0)t} e^{-\Gamma_f t - \Gamma_w^2 t^2} c(t), \tag{6}$$

of the auto-correlation function

$$c(t) = \langle \Psi(0) | \Psi_f(t) \rangle, \tag{7}$$

of the integrated core-excited $|\Psi(0)\rangle$ and final state $|\Psi_f(t)\rangle$ wave-packets, defined as:

$$|\Psi_f(t)\rangle = e^{-\imath h_f t} |\Psi(0)\rangle, \quad |\Psi(0)\rangle = \int_0^\infty dt_1 e^{-\Gamma t_1} e^{\imath(\Omega+\Delta)t_1} |\Psi_c(t_1)\rangle. \tag{8}$$

The core-excited nuclear wave packet $|\Psi_c(t)\rangle$ is computed using (5). In our case, the final electronic state is the ground state, so that $f = g$. The lifetime of the final state $\Gamma_f^{-1} \equiv \Gamma_0^{-1}$ is the vibrational lifetime which is incomparably larger (milliseconds) than the typical time of the wave packet dynamics (femtoseconds). Due to this, in our numerical simulations (6) we use a Gaussian window function of half-width at half maximum $\Gamma_w = 0.036$ eV, which allows to significantly decrease the computation time yet resolving all necessary spectral details. We note that the window function – the only source of RIXS spectral broadening in our simulations – is much smaller as compared to the experimental instrumental broadening presently available (≤ 0.1 eV [15]). In (6), P_f factor is defined by the experimental geometry and the symmetry of the final state. This factor only changes the absolute value of the cross section not affecting vibrational effects discussed here, thus we use $P_f = 1$ in our calculations. As we start the transition from the higher ground vibrational states it is obvious that in the RIXS profile we will see anti-Stokes lines, corresponding to emission processes to the lower vibrational levels of the electronic ground state.

D. X-ray absorption in the Raman scattering mode

As already discussed in the Introduction, there are different available methods for selective population of vibrational levels [17–20]. We note that in conventional schemes, the pump IR field usually populates several vibrational levels $|\psi_{s,a}\rangle$ with the population weight $\rho_{s,a}$, implying that an IR-pump - X-ray probe experiment measures the cross section as a sum of

particular absorption profiles from individual vibrational states:

$$\sigma_{\rm abs}(\omega) = \sum_{\nu} \rho_\nu \sigma_\nu(\omega), \quad \nu = (s,a), \tag{9}$$

where the partial XAS cross section can be written using Fermi's golden rule in time-independent representation

$$\sigma_\nu(\omega) \propto \sum_{\nu_c} \frac{|\langle \psi^c_{\nu_c} | \psi_\nu \rangle|^2}{(\Omega + \Delta - \epsilon_c)^2 + \Gamma^2}, \tag{10}$$

where $|\psi^c_{\nu_c}\rangle$ ($\nu_c = (s,a)$) is the 2D vibrational wave functions of the core-excited electronic state, and ϵ_c is the vibrational energy of the state $\nu_c = (s,a)$. Apparently, the partial cross section (10) can not be measured using a conventional XAS experiment. However, the RIXS technique gives us a unique opportunity to measure the XAS absorption $\sigma_\nu(\omega)$ from certain initial vibrational states $\psi_{s,a}$. The idea to measure XAS in the resonant x-ray scattering mode was implemented successfully to get the XAS profile of CO system with extremely high resolution [21] using resonant Auger measurements. In the present paper, we propose to apply this technique for the RIXS scheme. Indeed, we can expect that the cross section in the scattering mode will coincide with the conventional XAS profile when $\omega = \omega'$. In order to obtain partial XAS $\sigma_\nu(\omega)$ in the Raman mode (XASRM) we need to measure the RIXS cross section $\sigma(\omega', \omega)$ as a function of excitation energy ω for the energy loss $\omega - \omega' = 0$. In this case, the RIXS cross section reads very similar to the XAS cross section (10)

$$\sigma(\omega, \omega' = \omega) \propto \left| \sum_{\nu_c} \frac{|\langle \psi^c_{\nu_c} | \psi_\nu \rangle|^2}{\Omega + \Delta - \epsilon_c + \imath\Gamma} \right|^2 . \tag{11}$$

One should notice, however, two differences between the XASRM (11) and conventional XAS (10) cross sections. First, the XASRM cross section is proportional to the 2nd power of the Franck-Condon factors, which results in a sharpening of the vibrational resonances. Second, the XASRM cross section contains a lifetime vibrational interference (LVI) contribution (interference term), which is not present for conventional XAS $\sigma(\omega)$ (10). As we will show with the help of numerical simulations, the influence of the LVI is though rather small (see Sec. III C).

III. RESULTS AND DISCUSSION

In the present paper we focus on simulations of the XAS and RIXS spectra when the initial vibrational state of the water molecule is prepared by a preceding IR pulse. In

what follows, we consider the six initial vibrational states $\psi_{s,a}$ of the electronic ground state $(s,a) = (00),(10),(01),(20),(11),(02)$ (shown in order of increasing energy). The incident photon energy ω is tuned near the resonances with the two lowest core-excited states of water molecule having dissociative $4a_1$ and bound $2b_2$ character. We use a two-step theoretical approach. First, we computed the 2D PESs of the ground and core-excited states (Fig.1(b)) using the RASSCF method followed by the second-order perturbation theory method RASPT2 implemented in the MOLCAS package [28]. The *ab initio* PESs were further used for the time-dependent solution of the 2D Schrödinger equation and spectral simulations, as explained in Sec. II, employing the locally developed eSPec program [9, 11].

A. X-ray absorption

The theoretical XAS profiles around the dissociative $4a_1$ and the bound $2b_2$ states are shown in Figs. 2 and 3, respectively, for six initial vibrational excited states of the molecule $\psi_{00},...,\psi_{02}$. In the case of the dissociative state we compare the XAS formation for the symmetric H_2O and non-symmetric HDO molecules. All *ab initio* x-ray absorption spectra were slightly shifted (≤ -0.1 eV) in order to fit the experimental energy positions [13, 26] measured for the case of the ground vibrational level ψ_{00}.

1. Reflection principle and vibrational wave function mapping

The overall shape (envelope) of the absorption profiles can be easily explained using the so-called reflection principle, well known in the photoelectron spectroscopy [2, 16], resonant Auger scattering and RIXS spectroscopy [31, 32]. In a very similar way it can be applied here to XAS. Indeed, as it is illustrated in Fig. 4 the x-ray absorption profile results from the projection of the initial vibrational function on to the potential energy curve of the core-excited states. The reflection principle can be easily understood when considering the dissociative core-excited state. The transitions to the classical turning point (vertical transition) produces absorption intensity which is proportional to the correspondent value of the ground state vibrational wave function. Thus the XAS profile reproduce approximately the square of the initial vibrational function. The accuracy of the reflection procedure depends on the slope $V_R = -dV/dR$ of the core-excited potential energy curve. In the one-dimensional case

the reflection principle has a simple graphical interpretation (Fig. 4). Indeed, Fig. 4 is quite self-explanatory that the single maximum lowest vibrational wave function produces a single peak structure in XAS, while the square of the vibrational wave function having two maxima results in a double peak in the XAS spectrum. A typical synchrotron radiation consists of a train of nanosecond pulses, much shorter that the vibrational lifetime (milliseconds). Due to this circumstance, the questions of decoherence and time-delay between the IR and x-ray pulses can be omitted here.

The technique of a simple geometrical interpretation can be applied to the bound core-excited states as well. For a clear reflection on the potential slope in this case, the potential minimum must be considerably shifted relative to the ground state minimum. For the bound state, the vibrational structure may appear on the top of the broad structures related to the shape of the initial vibrational wave function. The vibrational structure is formed according to the Franck-Condon amplitudes and changes when the initial vibrational wave function (IVWF) is changed. In the 2D case studied here it works in a very similar way, however, its graphical interpretation becomes rather complicated. Let us describe how the reflection principle in 2D allows to map the structure of the initial vibrational wave function.

In order to understand the XAS formation in the 2D case, let us first analyze the PES of the ground and core-excited states. As one can see from Fig.1, the potentials are symmetric along the symmetric stretching mode $Q_s \sim R_1 - R_2$. This fact has crucial impact on the XAS formation and can be understood when the symmetry of the IVWF is also considered. In the simplest case of ψ_{00} an IVWF single peak XAS profile is produced by mapping the shape of the square of the IVWF (Fig.2). It is here easy to associate the double maximum structure of the ψ_{10} IVWF with the double peak of the XAS spectrum. However, the excitation from the ψ_{01} IVWF, having two maxima, results in a single peak XAS. This can be understood when considering the transition energy from the ground to core-excited state PES near the two maxima of the IVWF. Due to the symmetry of the core-excited potential, the energies related to the two maxima are the same resulting in a degeneracy of the XAS peak. We note that when the reflection symmetry of the PES is broken, as it is the case for HDO molecule, the degeneracy is lifted and a two peak XAS profile is observed.

XAS profiles for HDO were also computed and presented for comparison (see red lines in Fig.2). In general, lifting of the molecular symmetry results in an observable change of the XAS profile in the case of HDO molecule, due to the different distribution of the ground

state IVWF. For the ψ_{02} initial state a three peak XAS is expected, which, however, is not completely resolved in H_2O due to the rather close energy positions of the peaks. In HDO, the three-peak structure manifestation in XAS is rather clear. Following a similar logic the formation of the XAS for the higher IVWF shown in Fig. 2 can be easily explained.

The $2b_2$ state has a bound character. Contrary to the smooth XAS profile in the case of the dissociative state, the XAS profile of the bound core-excited state clearly shows vibrational structure. The positions of the vibrational levels of the core-excited state is shown by the thin green lines - a Franck-Condon factor analysis and a state assignment are also presented in Fig. 3. The envelope of the XAS spectrum satisfies the same tendency that was explained for the dissociative state. For the excitation of the initial ψ_{00} we can discern only a rather small range of the vibration transitions limited by the Frank-Condon region. In order to increase the FC area higher initial vibrational levels have to be considered. This results in a broader XAS profile with more vibrational states excited as can be seen from Fig. 3. This is very important for a more accurate mapping of the core-excited potential. It shows how the IR-excitation of the ground state and the following excitation of the system with x-rays give the possibility to scan the PESs of molecular core-excited states, thereby manipulating the dynamic processes in simple molecules.

2. Selection rules and mode separation

In the bound-to-continuum transition to the $4a_1$ core-excited state, no selection rules are manifested. Indeed, ground state eigenfunctions of any symmetry have non-zero overlap with the continuum wave function. However, in the case of the bound-to-bound transition symmetry selection rules are clearly observed from Fig. 3. Let us discuss now how the symmetry selection rules in XAS from the vibrationally excited molecule can be used for mode separation and mapping of the bound core-excited PES along the coordinates of particular vibrational modes. Let us start with the analysis of the wave function symmetry in the ground and core-excited states. The important feature of the PESs of these states is that they have reflection symmetry relative to the $Q_s \approx R_1 - R_2$ axis. This potential characteristic defines the symmetry of the vibrational functions, which are either symmetric or antisymmetric with respect to the reflection along the Q_s coordinate. In the harmonic approximation, the 2D vibrational wave function can be written as a product of the 1D wave

functions:

$$\psi_{s,a}(Q_s, Q_a) \approx \psi_s(Q_s)\psi_a(Q_a). \tag{12}$$

The harmonic approximation is valid for the lower vibrational states, and breaks down for the high vibrational excitation where the PES of the ground and core-excited states become strongly anharmonic (see Fig. 1). In the case of the harmonic approximation, the symmetry of the total 2D wave function is defined by the wave function of the antisymmetric mode $\psi_a(Q_a)$

$$\psi_a(-Q_a) = (-1)^a \psi_a(Q_a). \tag{13}$$

This symmetry rule is illustrated by the shape of the few lowest 2D wave functions for the ground (Fig. 2, right panel) and $2b_2$ core-excited (Fig. 5) states. Taking into account that the partial XAS probability (10) defined by the overlap of the vibrational wave functions of the ground and core-excited state, one can easily conclude that starting from the symmetric ground state wave function ψ_{00} only the symmetric stretching mode progression can be excited in the XAS. This is clearly confirmed by the XAS spectrum with Franck-Condon analysis presented in the Fig.3. The only way to reach the antisymmetric mode excitation in the core-excited state is to use initially excited antisymmetric stretching state in the ground state. Indeed, when the molecule in the excited antisymmetric state ψ_0 absorbs an x-ray photon, the XAS profile contains a progression (01),(11),(21),... related to the excitation of the first antisymmetric quantum in the core-excited state. The same vibrational progression is excited in the case of the ψ_{11} initial state. In this case, however, the envelope of the spectral profile is different, reflecting the shape of the IVWF (see Fig.4). Using even higher excited vibrational states allows to trace higher antisymmetric vibrational states in the XAS, as is seen from Fig. 3 (see cases ψ_{20}, ψ_{02}). Indeed, for both the ψ_{20} and ψ_{02} initial states the higher antisymmetric vibrational levels $a > 1$ can be reached.

Let us note that due to strong anharmonisity of the PESs, the symmetry section rules are here combined with the propensity selection rule defined by the shape of the vibrational wave functions. In the ground state, the symmetric and antisymmetric vibrational levels are nearly degenerate, and thus forms groups with nearly the same energy related to the total vibrational quantum number $n = s + a$. The stretching modes are strongly coupled (Darling-Dennison coupling), which sufficiently modifies the shape of the wave functions as compared to the ones in harmonic approximation[6]. Moreover, due to the anharmonicity

the higher ground vibrational states are not distributed symmetrically and have the tendency to bifurcate [24]. In the core-excited bound $2b_2$ state, in contrast, the symmetric and antisymmetric modes are well separated, as it is suggested by the PES shape (Fig. 1). We can clearly see from Fig.3 a strong difference in the quanta of the symmetric (0.186 eV) and antisymmetric (0.444 eV) modes. Due to this fact, the core-excited vibration states do not show the same grouping as in the ground state. Fig.5 shows that for the lower vibrational states the core-excited wave functions are localized mainly along the symmetric coordinate, reflecting the shape of the PES. For the higher excited states, however, quasi-degeneracy of the vibrational energies and coupling of the vibration states is found. For example, the quasi-degeneracy of ψ_{50}, ψ_{21} and ψ_{02} results in significant disturbance of the shape of wave function (Fig.5).

The results presented above clearly show that the symmetry selection rules together with the propensity rules provide selective vibrational excitation observed in the XAS profile. The use of initially excited vibrational states allows to manipulate the excitation of a particular vibrational mode in the core-excited state. In particular, the XAS from the vibrationally excited molecule can be used for the mapping [33] of the core-excited PES along particular (symmetric or antisymmetric) stretching modes in symmetric systems.

B. RIXS from vibrationally excited molecules

RIXS is a well established technique for probing of the electronic ground and valence excited states of the neutral molecules. Here we consider a particular case of the RIXS, namely electronically elastic x-ray scattering back to the ground state, the so-called "quasi-elastic" scattering channel. Due to nuclear dynamics in the core-excited state, a vibrational progression is usually observed in RIXS to the ground state, which allows to study the ground state potential along particular modes [8]. In the present section we will discuss RIXS from vibrationally excited molecules. The RIXS spectra here are computed for the excitation energy tuned into the resonance with the lowest vibration level $\nu_c = (00)$ in the case of the bound $2b_2$ core-excited state, and to the vertical transition energy in the case of dissociative $4a_1$ core-excited state.

In RIXS, similar to the x-ray absorption process, the reflection principle can be employed for analysis of the spectra [32]. In the present case, the core-excited wave-packet shape is

reflected on the ground state PES in terms of a change of the spectral envelope. For example, the core-excited wave packet in the dissociative state propagates fast towards the long bond-length range, which results in a wide vibrational progression in the $4a_1$ RIXS band up to 6 eV energy loss. In contrast, the core-excited wave packet on the $2b_2$ state is confined to a rather short bond length, and thus only a relatively short vibrational progression is observed in this case. The dependence of the spectral envelopes on the initially excited vibrational state is also observed (see Fig. 6) as a result of the change of the shape of the core-excited wave packet.

In a conventional RIXS transition to the ground electronic state, the lowest vibrational level appears at zero energy loss and corresponds to the totally (electronically and vibrationally) elastic scattering channel (see Fig.6, upper plot). Here we consider scattering starting from the excited vibrational level. When the final vibrational level is lower than the initial one, it results in the emission of a photon of higher energy than absorbed one, the so-called anti-Stokes, having negative energy position in the energy loss scale $\omega - \omega'$. From Fig.6, one can see that RIXS starting from the $n = 1$ group results in one anti-Stokes line, which corresponds to the transition to the ψ_{00} state.

Symmetry selection and propensity rules can also be applied to RIXS spectra. In conventional RIXS, starting from the ground vibrational level, the symmetry selection rule allows scattering only to the even vibrational states of the antisymmetric stretching mode $a = 0, 2, ...$ As it was discussed in [15] the selection and propensity rules manifested in the RIXS profile of water and open the possibility for selective gating of the stretching mode. In the case of RIXS from a vibrationally excited molecule the selection rules are modified accordingly to the symmetry of the initial vibrational state. For example, one can see that the anti-Stokes line is forbidden in RIXS from ψ_{01}. Indeed, the initial antisymmetric vibrational wave function ψ_{01} does not allow for transitions to the pure symmetric final state ψ_{00}. A similar situation is observed in the case of the antisymmetric initial wave function ψ_{11} (see Fig. 6). The second (elastic) peak in the RIXS spectra from the initial states of the $n = 1$ group (ψ_{10}, ψ_{01}) corresponds to the transition to the $n = 1$ group of two nearly degenerated final vibrational states ψ_{01} and ψ_{10}. Due to this fact, this resonance can be observed for both initial symmetric and antisymmetric states (e.g. ψ_{01} and ψ_{10}). However, in the case of the initial ψ_{10} (ψ_{01}) state only the symmetric (antisymmetric) component of the doublet $n = 1$ is allowed. In the case of RIXS starting from the initial vibrational group with $n = 2$

two anti-Stokes lines may appear – corresponding to transitions to the $n = 0$ and $n = 1$ final level groups. Similarly to the initial $n = 1$ states, in the case of the antisymmetric ψ_{11} state the anti-Stokes line for the transition to ψ_{00} is forbidden for the both the intermediate $4a_1$ and $2b_2$ states.

The quasi-degeneracy of the vibrational states results in fine structure in the RIXS spectra which is strongly dependent on the initial vibrational state, since reflection symmetry of the wave function has to be preserved. This fact is illustrated in Fig. 7 where a zoom-in on the RIXS spectra in the 0-2 eV interval is shown. The Franck-Condon analysis presented by the colored bars were computed as an overlap of the integrated core-excited wave packet with the ground state vibrational wave functions $\langle\Psi(0)|\psi_{s,a}\rangle$. The reflection symmetry of the core-excited wave packet is defined by the symmetry of the initial vibrational functions, which results in the selection rules for the RIXS channels. This selection rules are, however, strict only for the lowest levels, were the PES can be considered as harmonic (Fig. 7). Due to the anharmonisity of the potential, the selection rules are modified by propensity rules for the higher vibrational levels, reflecting the difference in shape of the PESs of the core-excited and final states of RIXS. For higher vibrational states in the RIXS progression the difference between $4a_1$ and $2b_2$ intermediate states becomes obvious (Figs. 6, 7), relating to the change of the fine structure due to the change of the shape of the core-excited wave packet. The propensity rule is much stronger in the case of the bound $2b_2$ state, since the eigenfunction of this state differs significantly from the ground state wave function. Indeed, in the case of the dissociative state, the selection rules are clearly preserved up to group $n = 5$ (see Fig. 7), while the RIXS spectrum via the $2b_2$ state demonstrates excitation of the mixed quanta ψ_{12}, ψ_{22}.

C. XAS measured in the Raman mode

As discussed above (see Sec. II D), in the case when selective population of an individual vibrational level of the ground state can not be reached the experimental XAS profile will show the sum of the cross-sections from different vibrational states weighted with their populations. In order to obtain an individual XAS profiles (10), we propose here to apply XAS measurements in the x-ray Raman scattering mode (XASRM, see Sec. II D). The vibrational structure of the $2b_2$ bound state allows for a rather detailed comparison between

XASRM and XAS. In order to investigate XASRM, we computed the RIXS maps by scanning the incident photon energy in a broad range across the $2b_2$ resonance for the two initial vibrational states ψ_{00} and ψ_{10} (Fig. 8). A horizontal cut of the maps corresponds to a RIXS spectrum at a particular incident photon energy. As was discussed in Sec. II D, the XASRM spectra can be obtained following the main diagonal of the RIXS map, where $\omega = \omega'$. One can see clearly that the intensity on the diagonal $\omega = \omega'$ in the left (right) plot strongly reminds of the squared x-ray absorption profile for the initial level ψ_{00} (ψ_{10}) (Fig. 3). As already mentioned, the XAS profile (10) is proportional to a square root of the XASRM profile (11). Square root of the diagonal cuts of the RIXS maps in Fig. 8 are presented in Fig. 10 together with the XAS profiles which clearly illustrate the ability to measure XAS in RIXS mode. Let us note that the XASRM profile, proportional to squared Franck-Condon intensities, shows in general a better resolution as compared to conventional XAS. A slight deviation of the XAS and XASRM results from the LVI interference in the core-excited state contributing to the RIXS spectra. One should note, however, that in the case when both ψ_{00} and ψ_{10} are initially populated, the experiment measures a superposition of the two RIXS maps. In the present case of the water molecule, where XAS to the $2b_2$ state shows a rather long vibrational progression, the RIXS spectra from the two initial states partially overlap at the region $\omega \approx 535.7 \ldots 536.7$ eV, so only a lower energy part of the XASRM from ψ_{10} remains uncontaminated by the contribution from the ψ_{00} RIXS and thus can be measured using XASRM. We note that the vertical transition energy $\omega_{c0}^{\rm vert}$, which corresponds to the maximum of the XAS profile, becomes smaller for the higher initial vibrational levels of the ground state, thus the whole RIXS map is shifted to lower energies in an absolute scale. Indeed, for the group $n = 2$ initial states the first absorption peak appears at 534.8 eV, which is about 1 eV below the first vibrational resonance for the ψ_{00} excitation (see Fig. 3). Therefore, the XASRM band can be considerably shifted for the highly excited vibrational levels ($n \geq 3$) as compared to ψ_{00} XASRM and thus the profiles can be separated.

The RIXS maps plotted in a relative energy scale, using the detuning Ω and the energy loss $\omega - \omega'$, for the $2b_2$ and $4a_1$ intermediate states and three initial vibrational levels ψ_{00}, ψ_{10}, and ψ_{01} of the ground state, are collected in Fig. 10. In this case, obviously, the $\omega = \omega'$ band always coincides with zero energy loss, which does not allow to separate XASRM profiles from different initially populated states. However, as one can see from the RIXS maps, the incoming energy dependence of the intensity of each final vibrational state (see vertical

bands in Fig. 10) resembles the XAS envelope. Indeed, one can clearly see a splitting of the RIXS map into two bands with $\Omega \approx 0.9$ and -0.1 eV in the case of the ψ_{10} initial state. This behavior reflects the double peak structure of the XAS (see Figs. 2, 3). In the case of ψ_{00} and ψ_{01} initial levels the XAS spectrum consists of a single peak, in total agreement with the behavior of the RIXS maps. Moreover, the fine structure of the each individual band shows vibrational structure of the core-excited state. This partial XAS separation in XASRM can be obtained by following the RIXS intensity of different final vibrational states.

Let us consider the anti-Stokes line at negative excess energy, which appears for scattering from $n = 1$ initial vibrational levels to the $n = 0$ final vibrational state. This line is clearly separated from the elastic scattering channel $\omega = \omega'$. Furthermore, due to the symmetry selection rules, the anti-Stokes line is forbidden for the antisymmetric ψ_{01} initial state, allowing for a clear separation of the XAS contribution from the ψ_{10} initial state. The Frank-Condon factors for the XASRM on the elastic channel differ from the ones for the anti-Stokes line, which results in a slight change of the XASRM profile as compared to eq.(11)

$$\sigma(\omega, \omega' = \omega + \epsilon_{10}) \propto \left| \sum_{\nu_c} \frac{\langle \psi_{00} | \psi^c_{\nu_c} \rangle \langle \psi^c_{\nu_c} | \psi_{10} \rangle}{\Omega + \Delta - \epsilon_c + i\Gamma} \right|^2 , \tag{14}$$

where ϵ_{10} is the vibrational energy of the ψ_{10} state. The calculation of XASRM using the anti-Stokes line is illustrated in Fig. 10 (dashed line). In spite of some disagreement with the XAS profile, the XASRM spectra based on anti-Stokes line shows all the main features of the absorption spectra, as well as accurate positions of the vibrational resonances in the $2b_2$ core-excited state. Similarly, the anti-Stokes lines for higher initial vibrational levels $n > 1$ can be used to single out the partial XAS contribution from these states.

IV. CONCLUSIONS

We have presented a theoretical study of x-ray absorption (XAS) and resonant inelastic x-ray scattering (RIXS) spectroscopy applied to vibrationally excited molecules, using water as a demonstration case. We have shown the flexibility of the IR-pump - X-ray-probe method for advanced studies of symmetric molecules, where the symmetry of a selected initial vibrational state allows to address a particular vibrational mode in the core-excited state and therefore also in the final RIXS state. The excited vibrational wave function of the

ground electronic state is more broadly distributed over nuclear coordinates as compared to the lowest vibrational wave function located near the equilibrium bond length, which, according to the reflection principle, allows to study an extended energy range of the potential energy surfaces (PESs) of the core-excited and final states. Together with symmetry selected excitation, the studied pump-probe technique can be applied for multidimensional mapping along a particular direction – as it here was analyzed for the symmetric or antisymmetric modes of the water molecule. We have shown that XAS measured in x-ray Raman mode allows to obtain a partial spectrum initiated from a single vibrational level of the ground state. Some of the results for the pump-probe method applied to the symmetric water molecule were compared against calculations for the non-symmetric HDO molecule, showing how the selection rules then alter the XAS and RIXS spectra. The proposed technique can be applied for advanced symmetry resolved studies of polyatomic molecules and ground state vibrational excitation followed by x-ray absorption can also be used for controlling chemical reactions over transition state barriers, as well as ultra-fast fragmentation and isomerization processes in the short-living core-excited states.

ACKNOWLEDGEMENT

This work was supported by the Russian Science Foundation (Grant No.16-12-10109), the Knut and Alice Wallenberg foundation (Grant No. KAW-2013.0020), and the Swedish Research Council (VR). Numerical simulations were performed using Swedish National Infrastructure for Computing (SNIC).

---

[1] P. Maksyutenko, M. Grechko, T. R. Rizzo, and O. V. Boyarkin, Philosophical Transactions of the Royal Society A: Mathematical, Physical and Engineering Sciences **370**, 2710 (2012).

[2] G. Herzberg and K.-P. Huber, *Molecular Spectra and Molecular Structure: Constants of diatomic molecules* (Van Nostrand Reinhold, 1979) p. 716.

[3] M. Grechko, O. V. Boyarkin, T. R. Rizzo, P. Maksyutenko, N. F. Zobov, S. V. Shirin, L. Lodi, J. Tennyson, A. G. Császár, and O. L. Polyansky, The Journal of chemical physics **131**, 221105 (2009).

[4] F. Gel'mukhanov and H. Ågren, Physics Reports **312**, 87 (1999).

[5] V. Kimberg, T. Gejo, M. Oura, T. Tokushima, Y. Horikawa, H. Arai, S. Shin, and N. Kosugi, Physical Review A **85**, 032503 (2012).

[6] R. C. Couto, *Coupled electron-nuclear dynamics in inelastic X-ray scattering*, Ph.D. thesis, KTH, Sweden (2016).

[7] F. Hennies, A. Pietzsch, M. Berglund, A. Föhlisch, T. Schmitt, V. Strocov, H. O. Karlsson, J. Andersson, and J.-E. Rubensson, Physical review letters **104**, 193002 (2010).

[8] S. Schreck, A. Pietzsch, B. Kennedy, C. Såthe, P. S. Miedema, S. Techert, V. N. Strocov, T. Schmitt, F. Hennies, J.-E. Rubensson, and A. Föhlisch, Scientific reports **7**, 20054 (2016).

[9] F. F. Guimarães, V. Kimberg, V. C. Felicíssimo, F. Gel'mukhanov, A. Cesar, and H. Ågren, Physical Review A **72**, 012714 (2005).

[10] F. F. Guimarães, V. Kimberg, V. C. Felicíssimo, F. Gel'mukhanov, A. Cesar, and H. Ågren, Physical Review A **71**, 043407 (2005).

[11] V. C. Felicíssimo, F. F. Guimarães, F. Gel'mukhanov, A. Cesar, and H. Agren, .

[12] M. N. Piancastelli, A. Hempelmann, F. Heiser, O. Gessner, A. Rüdel, and U. Becker, Physical Review A **59**, 300 (1999).

[13] A. Hiraya, K. Nobusada, M. Simon, K. Okada, T. Tokushima, Y. Senba, H. Yoshida, K. Kamimori, H. Okumura, Y. Shimizu, A. L. Thomas, P. Millie, I. Koyano, and K. Ueda, Physical Review A - Atomic, Molecular, and Optical Physics (2001), 10.1103/PhysRevA.63.042705.

[14] P. Sałek, F. Gel'mukhanov, and H. Ågren, Physical Review A **59**, 1147 (1999).

[15] R. C. Couto, V. V. da Cruz, E. Ertan, S. Eckert, F. Fondell, M. Dantz, B. O'Cinneide, Schmitt, A. Pietzsch, F. F.Guimarães, H. Ågren, F. Gel'mukhanov, M. Odelius, V. Kimberg, and A. Föhlisch, to be published.

[16] R. Schinke, *Photodissociation Dynamics: Spectroscopy and Fragmentation of Small Polyatomic Molecules (Cambridge Monographs on Atomic, Molecular and Chemical Physics)* (1995).

[17] U. Gaubatz, P. Rudecki, S. Schiemann, and K. Bergmann, The Journal of Chemical Physics **92**, 5363 (1990).

[18] C. Leonard, G. Chambaud, P. Rosmus, S. Carter, and N. C. Handy, Physical Chemistry Chemical Physics **3**, 508 (2001).

[19] M. Becker, U. Gaubatz, K. Bergmann, and P. L. Jones, The Journal of Chemical Physics **87**, 5064 (1987).

[20] G. K. Paramonov and O. Kühn, Journal of Physical Chemistry A **116**, 11388 (2012).

[21] Y. Hikosaka, Y. Velkov, E. Shigemasa, T. Kaneyasu, Y. Tamenori, J. Liu, and F. Gel'mukhanov, Physical review letters **101**, 073001 (2008).

[22] L. Halonen, in *Advances in Chemical Physics, vol.104*, edited by I. Prigogine and S. A. Rice (1998) pp. 41–180.

[23] Michael E. Kellman, Annual Review of Physical Chemistry **46**, 395 (1995).

[24] M. E. Kellman and V. Tyng, "The dance of molecules: New dynamical perspectives on highly excited molecular vibrations," (2007).

[25] B. T. Darling and D. M. Dennison, Physical Review **57**, 128 (1940).

[26] Lothar Weinhardt, Andreas Benkert, Frank Meyer, Monika Blum, Regan G. Wilks, Wanli Yang, Marcus Bär , Friedrich Reinert and C. Heske, J. Chem. Phys. **136**, 144311 (2012).

[27] P. A. Malmqvist, A. Rendell, and B. O. Roos, The Journal of Physical Chemistry **94**, 5477 (1990).

[28] F. Aquilante, L. De Vico, N. Ferré, G. Ghigo, P.-A. Malmqvist, P. Neogrády, T. B. Pedersen, M. Pitonák, M. Reiher, B. O. Roos, L. Serrano-Andrés, M. Urban, V. Veryazov, and R. Lindh, Journal of computational chemistry **31**, 224 (2010).

[29] F. F. Guimarães, *X-ray spectroscopy of molecules driven by strong infrared fields*, Ph.D. thesis, KTH, Stockholm,Sweden (2006).

[30] V. V. da Cruz, R. C. Couto, , E. Ertan, S. Eckert, F. Fondell, M. Dantz, B. O'Cinneide, Schmitt, A. Pietzsch, F. F.Guimarães, H. Ågren, F. Gel'mukhanov, M. Odelius, V. Kimberg, and A. Föhlisch, to be published.

[31] F. Gelmukhanov and H. Ågren, Physical Review A **54**, 379 (1996).

[32] V. Kimberg and C. Miron, Journal of Electron Spectroscopy and Related Phenomena **195**, 301 (2014).

[33] N. K. Catalin Miron, Christophe Nicolas, Oksana Travnikova, Paul Morin1, Yuping Sun , Faris Gel'mukhanov and V. Kimberg, Nature Physics **8**, 135 (2012).

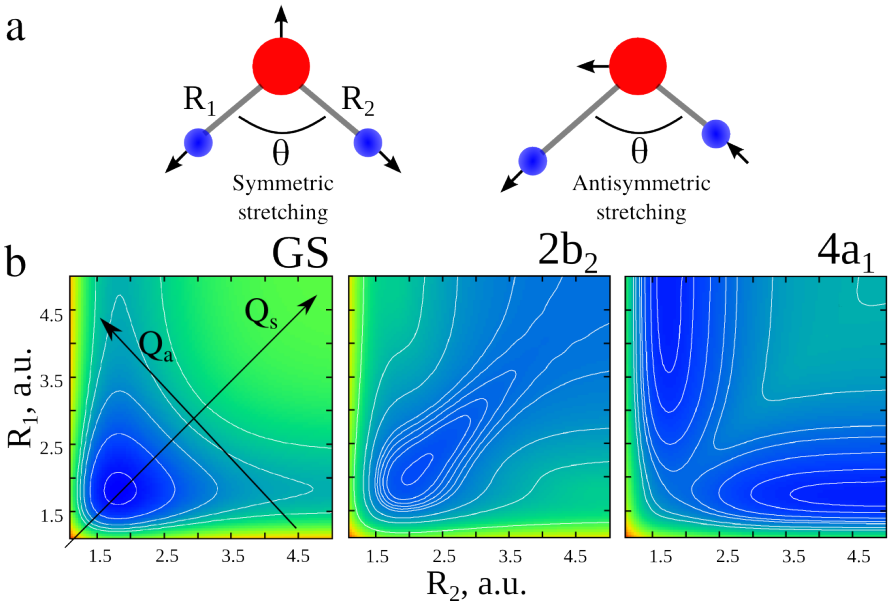

FIG. 1. (a) The stretching vibrational modes of the water molecule and valence coordinates representation. (b) 2D stretching mode potential energy surfaces of the ground state (GS) and two lowest core-excited states of water molecule (dissociative $4a_1$ and bound $2b_2$) in valence coordinates R_1, R_2. The directions of the normal symmetric Q_s and antisymmetric Q_a are also shown schematically.

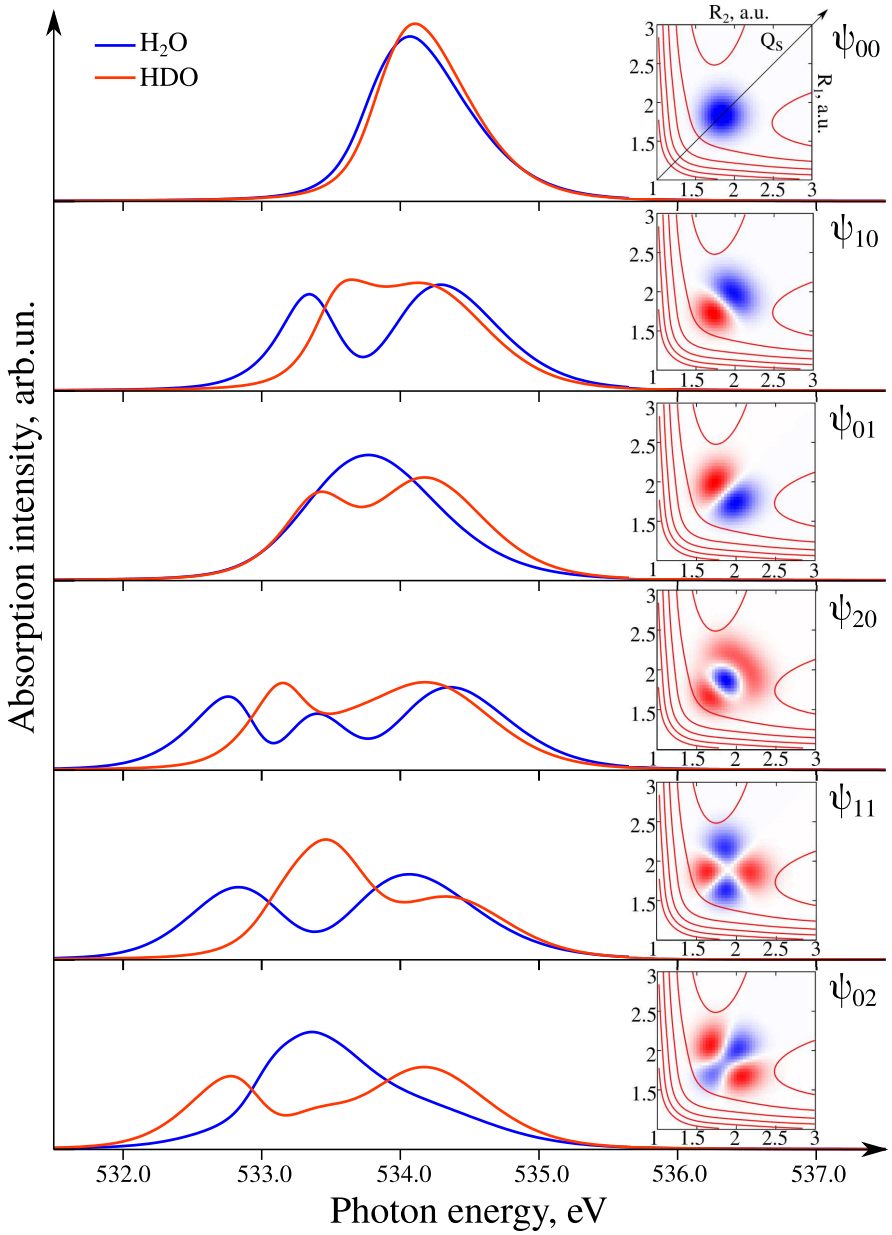

FIG. 2. Theoretical x-ray absorption spectra of gas phase H_2O (blue lines) and HDO (red lines) molecules at the dissociative $4a_1$ resonance. XAS from the six lowest vibrational levels are shown. The right-hand side panels present the initial vibrational wave functions of water together with the core-excited state potential of water drawn by the isolines. Red and blue parts of the wave functions describes positive and negative values, respectively.

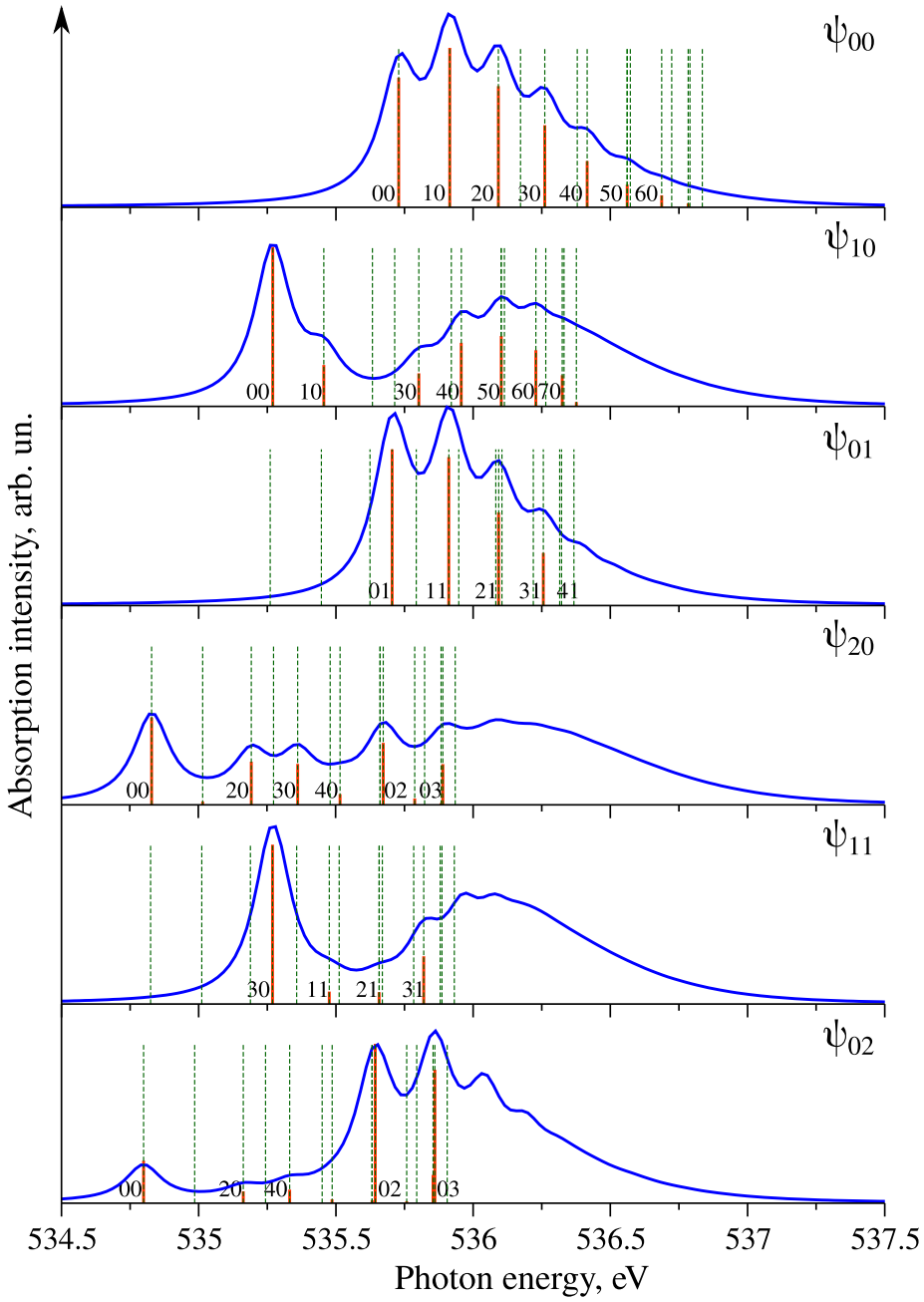

FIG. 3. X-ray absorption spectra of gas phase H_2O near the bound $2b_2$ core-excited state. Six lowest initial vibration states are denoted as $\psi_{s,a}$, and their vibrational wave functions are presented in Fig.2. Green dashed lines correspond to the core-excited vibrational energy levels. Calculated Franck-Condon factors are represented by the assigned red lines.

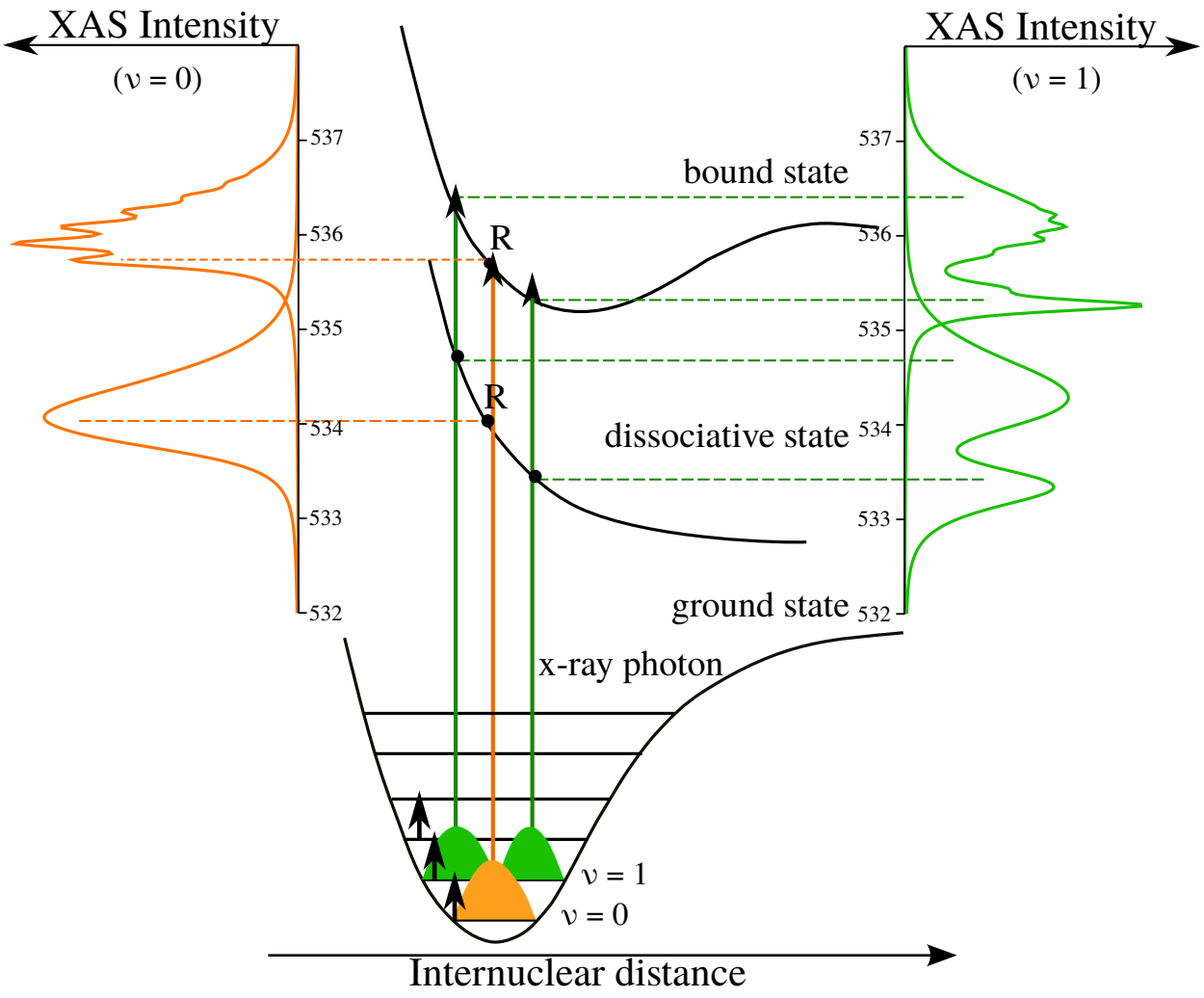

FIG. 4. Schematic representation of the ground state vibrational wave function mapping using the transitions to the continuum and bound core-excited states based on the reflection principle. XAS at the left-hand side shows excitation from the ground vibrational level, while XAS at the right-hand side shows excitation of the first excited vibrational state having one node.

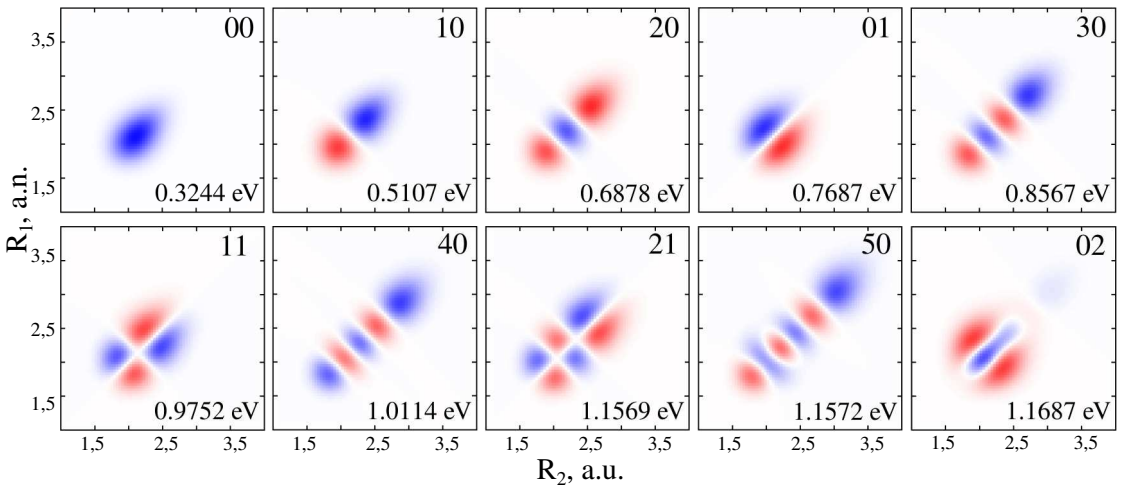

FIG. 5. The first ten vibrational eigenfunctions $\psi^c_{\nu_c}$ of the core-excited $2b_2$ state of H_2O. The plots are arranged (left-right, up-down) by increase of the vibrational energy (shown in the plots) and labeled with the 2D vibrational quanta numbers (s, a).

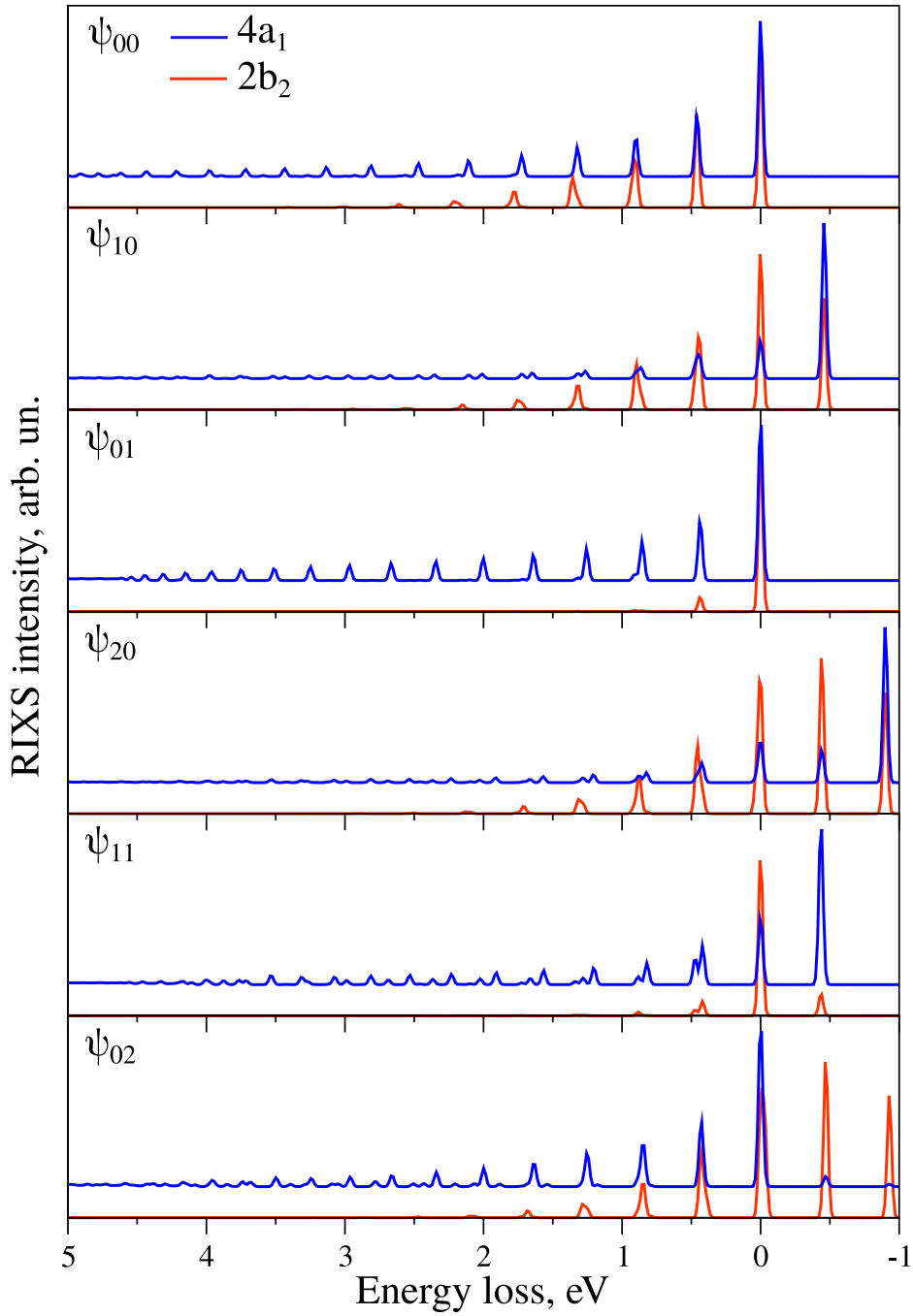

FIG. 6. Theoretical RIXS spectra of a vibrationally excited H_2O. The plots are marked with initial vibrational wave functions used in the RIXS simulations. The $4a_1$ RIXS spectra are shifted vertically for better visibility.

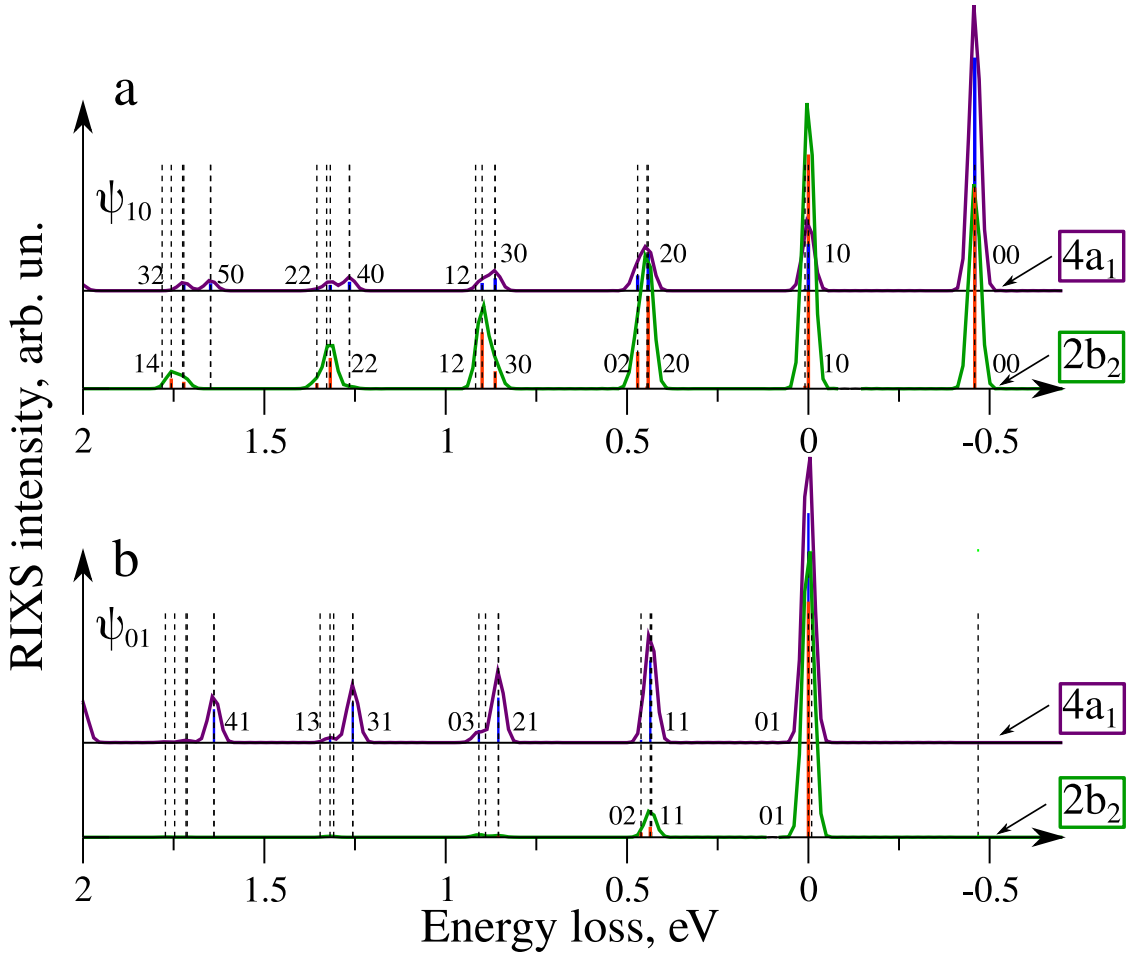

FIG. 7. Fine structure of the RIXS spectrum of H_2O molecule with initial vibrational state ψ_{10} and ψ_{01}. The dashed lines show the ground state eigenvalues. The blue and red lines show the Frank-Condon factors for the emission from $4a_1$ and $2b_2$ states, respectively. The allowed vibrational states are assigned.

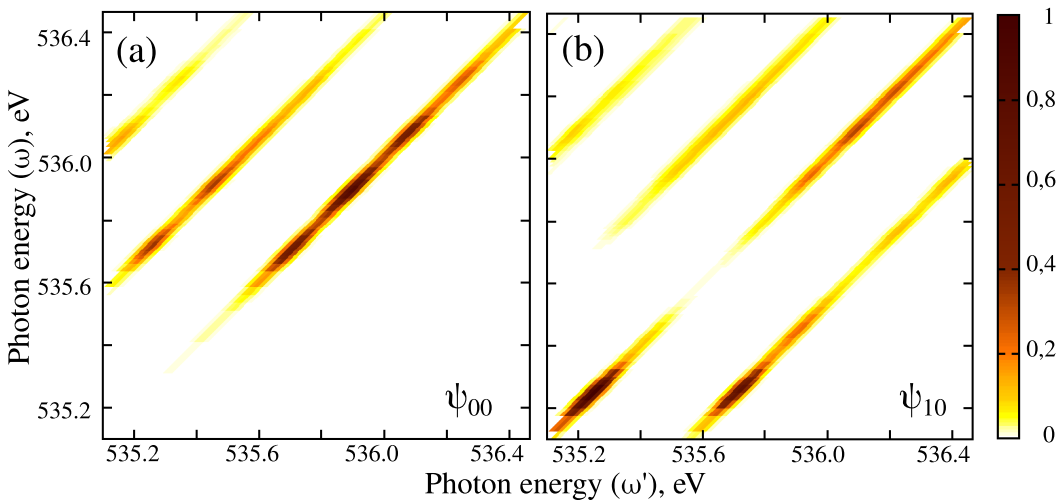

FIG. 8. RIXS maps for the scattering process from the initial (a) ψ_{00} and (b) ψ_{10} excited vibrational functions via the $2b_2$ core-excited state of H_2O. The absolute energy scale is used: incident vs. emitted photon energy. Each map is normalized to its maximal value.

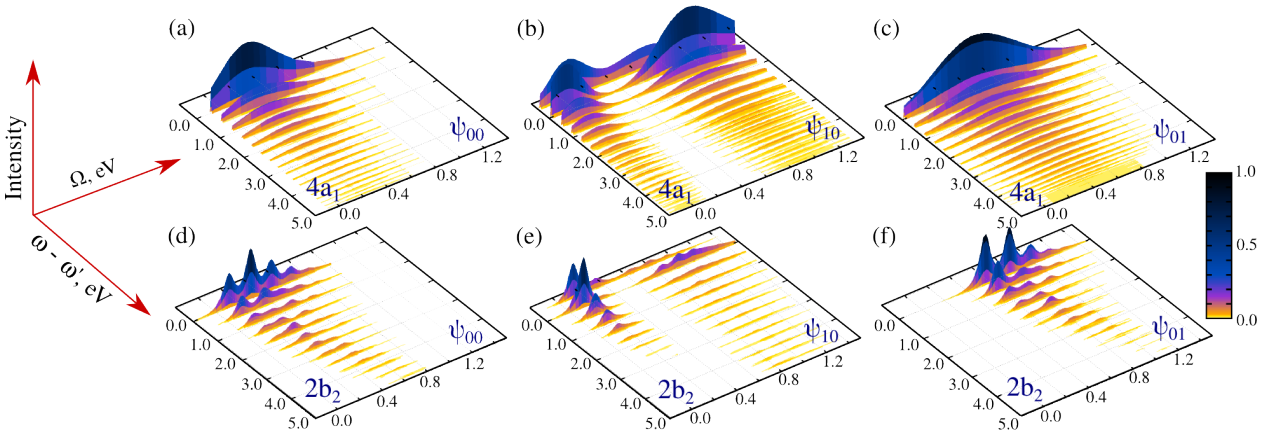

FIG. 9. RIXS 3D maps for the tree lowest initial states ψ_{00}, ψ_{10}, and ψ_{01} via $4a_1$ (a-c) and $2b_2$ (d-f) core-excited states of H_2O. The relative energy scale of detuning Ω vs energy loss $\omega - \omega'$ is used. All maps are normalized on their maximal value.

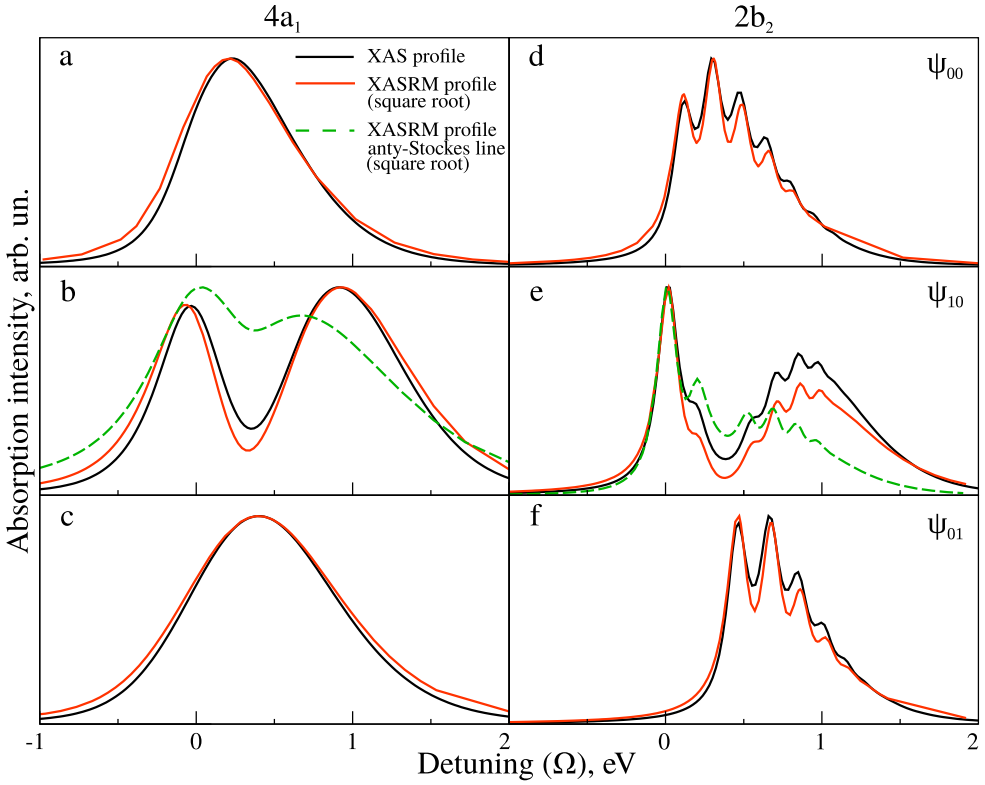

FIG. 10. XASRM spectra of H_2O molecule obtained from RIXS maps (Fig. 9) at fixed energy loss $(\omega-\omega')$ for $4a_1$ (a-c) and $2b_2$ (d-f) core-excited states. The ψ_{00} (a,d), ψ_{10} (b,e), and ψ_{01} (c,f) initial ground vibrational levels are used. The black line is the conventional XAS profile, while the red lines are the square root of the XASRM cross section (11) for $\omega-\omega'=0$. The green dashed line is the square root of XASRM profile found using the anti-Stokes line $\psi_{10}\rightarrow\psi_{00}$ (14) ($\omega-\omega'=-0.46$ eV). All spectra are normalized on their maximum values.